# Predicting the Influence of Microvascular Structure On Tumor Response to Radiotherapy

James A. Grogan*, Bostjan Markelc, Anthony J. Connor, Ruth J. Muschel, Joe M. Pitt-Francis, Philip K. Maini, and Helen M. Byrne

***Abstract*—*Objective:*** **The purpose of this study is to investigate how theoretical predictions of tumor response to radiotherapy (RT) depend on the morphology and spatial representation of the microvascular network.** ***Methods:*** **A hybrid multiscale model, which couples a cellular automaton model of tumor growth with a model for oxygen transport from blood vessels, is used to predict the viable fraction of cells following one week of simulated RT. Both artificial and biologically derived three-dimensional (3-D) vessel networks of well vascularized tumors are considered and predictions compared with 2-D descriptions.** ***Results:*** **For literature-derived values of the cellular oxygen consumption rate there is little difference in predicted viable fraction when 3-D network representations of biological or artificial vessel networks are employed. Different 2-D representations are shown to either over- or under-estimate viable fractions relative to the 3-D cases, with predictions based on point-wise descriptions shown to have greater sensitivity to vessel network morphology.** ***Conclusion:*** **The predicted RT response is relatively insensitive to the morphology of the microvessel network when 3-D representations are adopted, however, sensitivity is greater in certain 2-D representations.** ***Significance:*** **By using realistic 3-D vessel network geometries this study shows that real and artificial network descriptions and assumptions of spatially uniform oxygen distributions lead to similar RT response predictions in relatively small tissue volumes. This suggests that either a more detailed description of oxygen transport in the microvasculature is required or that the oxygen enhancement ratio used in the well known linear-quadratic RT response model is relatively insensitive to microvascular structure.**

***Index Terms*—Multiscale modeling, oxygen transport, radiotherapy (RT), vascular tumor growth.**

Manuscript received May 18, 2016; revised July 27, 2016; accepted August 4, 2016. Date of publication September 8, 2016; date of current version February 16, 2017. This work was supported in part by the European Union's Seventh Framework Programme for research, technological development and demonstration under Grant 600841, in part by the People Programme (Marie Curie Actions) of the European Union's Seventh Framework Programme through FP7/2007-2013 under REA Grant 625631, and in part by the Cancer Research UK (CRUK) through the CRUK Oxford Centre under Grant C5255/A18085. *Asterisk indicates corresponding author.*

*J. A. Grogan is with the Mathematical Institute, University of Oxford, Oxford OX2 6GG, U.K. (e-mail: grogan@maths.ox.ac.uk).

P. K. Maini and H. M. Byrne are with the Mathematical Institute, University of Oxford.

J. M. Pitt-Francis and A. J. Connor are with the Department of Computer Science, University of Oxford.

B. Markelc and R. J. Muschel are with the Department of Oncology, CRUK/MRC Oxford Institute for Radiation Oncology, University of Oxford.

Digital Object Identifier 10.1109/TBME.2016.2606563

## I. Introduction

IN *vitro* studies have shown that cancer cells in low oxygen environments have a greater probability of survival following radiotherapy (RT) than cells with greater oxygen availability [32]. This effect has been shown to translate to the clinic, with patients exhibiting markers for hypoxia having poorer RT response [5]. Oxygen availability in vascular tissue is closely linked with the function of the microvasculature and studies have focused on the measurements of vascular function [28] or microvessel density as indicators of RT responsiveness [11]. Important questions remain following these studies regarding the link between vascular structure, tumor tissue oxygenation, and RT response. In particular, observations of improved RT outcome when vascular targeting agents are administered [12], suggesting a temporal window during which the vascular structure can be optimized for tissue oxygenation as described by "vascular normalization" theory [13].

Mathematical models of vascular tumor growth and radiation therapy response can be used to study the link between indirect measurements of vascular structure, tissue oxygenation, and RT response. Dasu *et al.* [7], [8] have studied oxygenation profiles and RT response using planar tissue regions, a cellular automaton description of cells, and a point-wise description of vessels. Vessels were heterogeneously distributed and predictions of different forms of the well known linear-quadratic (L-Q) model of cell survival, with and without an oxygen enhancement ratio (OER), were compared. The OER is used to represent the decrease in sensitivity of cells in low oxygen environments to RT. Scott *et al.* [29] used a similar approach to study the effects of spatial heterogeneity in the distribution of vessels on cell survival post-RT. The authors predicted that microvessel density alone does not adequately describe average tissue oxygenation or RT response and proposed improved spatial descriptions of heterogeneity in vessel spacing.

Many existing modeling studies focus on the *in vitro* response of tumor spheroids to RT [14], while models of the *in vivo* response neglect the vasculature [9] or they focus on the macroscale behavior and neglect details of microvascular structure [26], [27]. Other authors have used detailed spatial descriptions of the microvascular network and oxygen transport processes to predict tissue oxygenation, without explicitly modeling cell response to RT [10], [23], [30], or they have adopted simplified or artificial descriptions of the vessel network and modeled cells discretely [16], [22], [24], [34]. The

present study aims to investigate RT response by retaining a discrete description of cell growth and treatment, while using realistic three-dimensional (3-D) representations of biological vessel networks of well vascularized tumors. It is desirable to use a discrete description of cell growth and treatment response as this permits a more mechanistic description of the multiscale vascular tumor growth process. In particular, the approach allows a natural description of oxygen dependent cell cycling and RT survival at the cell scale and the simultaneous development of spatial heterogeneities in oxygen tension and cell populations as the nutrient is delivered from aberrant tumor vessels at larger spatial scales. The ability to represent spatial heterogeneities in oxygen tension and cellular composition is important when studying tumor response to RT, as it permits investigation of the processes that give rise to phenomena such as improved RT response following "vessel normalization" and reduced responsiveness in hypoxic regions [12], [13].

In the present study a cellular automaton approach similar to those of Dasu *et al.* [7], Scott *et al.* [29], and Owen *et al.* [20] is used to simulate the growth of tumor cells. However, in this case a 3-D tissue volume is considered and vessels are described as line sources of oxygen, rather than points. In addition, both artificial vessel networks and vessel networks derived from imaging data from mouse tumors are adopted. The inclusion of *in vivo* data on vessel network structures allows us to assess the ability of previously adopted artificial networks and 2-D descriptions, to predict RT outcome.

The remainder of the study is organized as follows. In Section II, the vessel networks are introduced and methods for their construction are described. Then, the hybrid multiscale model of vascular tumor growth and cell response to RT is described and simulation test cases are introduced. In Section III, numerical results are presented, showing predicted oxygen distributions and cell populations for each vessel network. Then, cell surviving fractions following the administration of one week of fractionated RT are generated and compared for each network. In Section IV, the key results are discussed, together with suggestions for future work. The paper concludes in Section V with a summary of our findings.

## II. Methods

Predicted oxygen profiles and RT responses are compared for simulated tumors with three different vessel networks, each with three different spatial representations. The networks are first introduced. Following this, the submodels of cell cycle progression and growth, oxygen delivery and consumption, and radiation response are described. Finally, the algorithm used to generate numerical simulations is presented. All spatial dimensions are scaled relative to an assumed cell width, $\Delta x$, of 40 $\mu$m, as per Owen *et al.* [20].

### A. Vessel Networks

Three vessel networks are studied, as shown in Fig. 1. The first, denoted "Regular," is an artificial 2-D regular hexagonal tessellation of a rectangular domain of dimension 40 $\times$ 40 cell widths. The network is positioned in the middle of a cuboidal domain with a depth of 7 cell widths. This network has previously been used in several studies of tumor growth and treatment [2], [3] and can be considered to represent a spatially homogeneous capillary bed. Three different spatial descriptions are studied; "Slice," "Planar," and "3-D." The "3-D" description is obtained by randomly choosing the out-of-plane location of network branch points from a uniform distribution bounded by the domain depth. The "Planar" description is obtained by projecting the network back onto the 2-D rectangular domain and the "Slice" description is obtained by intersecting the "3-D" description with the domain mid-plane. The intersection produces a collection of points and closely resembles the description of Dasu *et al.* [7] and Scott *et al.* [29].

The second network, denoted "Random," is a 2-D Voronoi tessellation bounded by a rectangular domain and with a uniform

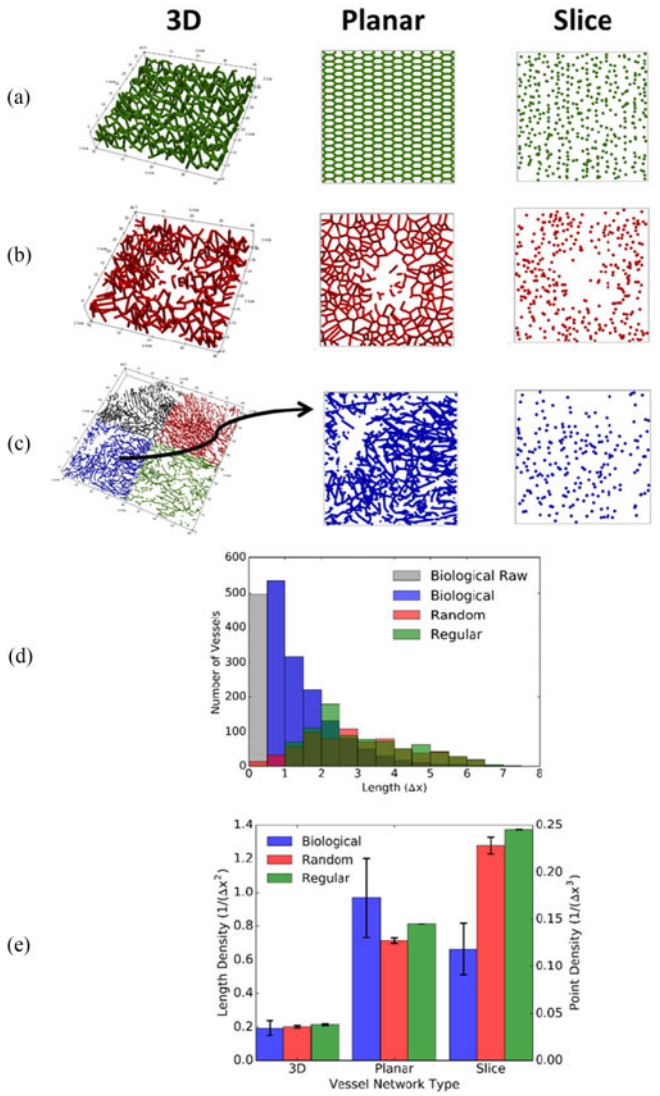


Fig. 1. Types of 3-D and 2-D vessel networks considered in this study. Plots show artificial networks with (a) "Regular" and (b) "Randomly" spaced vessels and (c) "Biological" networks, with 3-D and 2-D "Planar" and "Slice" representations. (d) Distribution of vessel lengths for the 3-D networks. "Biological Raw" is the distribution before short vessels removal. (e) Average length density for the 3-D and 2-D "Planar" networks, and the average point density of vessels for the 2-D "Slice" networks. Error bars denote one standard deviation, with artificial networks generated using different random seeds and the biological network divided into four sub-networks.

spatial distribution of point seeds. For the "3-D" description, vessel branch locations are perturbed randomly in the out-of-plane direction to fill the cuboidal domain. Following this, points are randomly selected from a normal distribution with mean centered at the domain midpoint. The closest vessels to these points are progressively removed until a target density is reached. The result, shown in Fig. 1(b), leads to a heterogeneous spatial distribution of vessels, with lower vessel density towards the center of the domain. The "Planar" and "Slice" descriptions are obtained as previously described.

The third network, denoted "Biological," is derived from a multiphoton image of a fluorescently labeled vessel network in a mouse tumor, as in Grimes *et al.* [10]. Briefly, murine colon adenocarcinoma (MC38) cells were cultured in Dulbecco's Modified Eagle Medium supplemented with 10% fetal bovine serum and 1% penicillin/streptomycin at 37 °C in a humidified incubator with 5% $CO_2$. Tumors were induced by injecting $0.5 \times 10^6$ cells in 100 $\mu$L 1× phosphate buffered saline, injected subcutaneously onto the right flank of a 8–10 weeks old female C57/Bl6 mice (Charles River). When the tumor reached approximately 200 $mm^3$ in volume (calculated as length×width× height× $\pi/6$) anti-mouse CD31 PE labeled antibodies, specifically labeling endothelial cells, were injected intravenously (25 $\mu$g in 100 $\mu$L, BioLegend) to label perfused blood vessels. Mice were culled and tumors excised, cut in half and imaged 10 min after injection of labeled antibodies in a humidified chamber with a cover glass bottom with thickness of 0.17 mm. Images were acquired with a Zeiss LSM 880 microscope (Carl Zeiss AG), connected to a Mai-Tai tunable laser (Spectra-Physics). Tumor tissue was excited with laser wavelength of 800 nm and the emitted light was collected on a Gallium Arsenide Phosphide detector through a 562.5–587.5 nm band-pass filter for PE. A 20× water immersion objective with NA of 1.0 was used to acquire Zstacks-TileScan of a random region in the center of tumor tissue with a pixel size of 0.83 $\mu$m in X and Y and a Z step of 2 $\mu$m. All animal studies were performed in accordance with the Animals Scientific Procedures Act of 1986 (U.K.) and Committee on the Ethics of Animal Experiments of the University of Oxford.

Following acquisition, image stacks were resized using bilinear interpolation in ImageJ [1] with pixel sizes increased by a factor of 4 in X and Y and 2 in Z. This operation facilitated later processing and also reduced noise. The channel containing the vessel label was converted to an 8-bit grayscale format and a binary mask was generated using thresholding with manual selection of upper and lower bounds (voxel intensities of 255 and 51, respectively). Vessel center-lines were obtained from the mask using the Skeletonize3D "plug-in for ImageJ." Small vessels, with length $< 0.5\Delta x$, were removed from the network as they were deemed to be artifacts of the center-line extraction. Vessel length distributions before and after removal are shown in Fig. 1(d). The network dimensions are $80 \times 80 \times 7$ cell widths, and the domain is divided into four, equally sized sub-networks [see Fig. 1(c)]. Subdivision is primarily for computational purposes, but also allows comparison of results in subregions of biological networks with different vessel distributions. Each sub-network is analyzed individually and subject to the same "Planar" and "Slice" operations as the "Random" network.

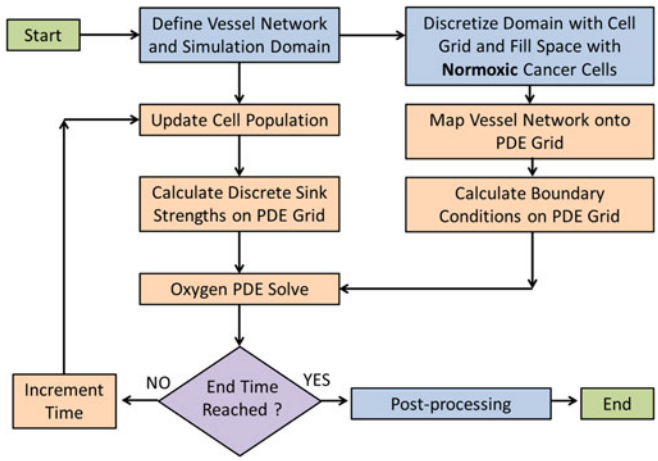


Fig. 2. Flowchart of the algorithm used in numerical simulations of the hybrid, multiscale model of tumor growth and response to RT.

Vessel length density distributions are shown for the "Biological" network, each sub-network and a sample of the artificial networks in Fig. 1(d). It is noted that the number of short vessels is greater in the biological networks than the artificial ones although, as shown in Fig. 1(e), average line densities are similar. It is also shown in Fig. 1(e) that line density increases significantly when a 2-D "Planar" representation is adopted. There is a significant variation in point density between the biological and artificial networks when the 2-D "Slice" representation is adopted, with the density being lower for the biological networks. This is due to the anisotropy of the biological network, which is not captured by the artificial networks and suggests that for this morphology multiple slices may need to be employed for point-based descriptions. The most suitable method for generating such slices is not considered in the present study, but the effect of the reduced point density due to using a single slice is investigated.

### B. Model Overview

The multiscale model of tumor growth and radiation treatment response adopted in this study is shown in Fig. 2. Cells are modeled discretely, using a cellular automaton approach. Three cell states are considered, "Normoxic," "Quiescent," and "Apoptotic." In a preprocessing step, a regular grid of spacing equal to an assumed (biological) cell spacing of $\Delta x$ is generated, filling the cuboidal simulation domain. All sites on the grid are populated with "Normoxic" cancer cells, except those occupied with a vessel. Vessels are described using a lattice-free approach, but vessel positions are interpolated onto the regular cell grid and the finite-difference grid used to solve the partial differential equation (PDE) governing tissue oxygen levels. The PDE governing tissue oxygen levels is of the form:

$$D_e \nabla^2 c - \delta(\mathbf{x}) k c = 0 \tag{1}$$

where $c$ is the oxygen tension, $D_e$ is the effective oxygen diffusion coefficient, and $k$ is the rate of oxygen consumption per

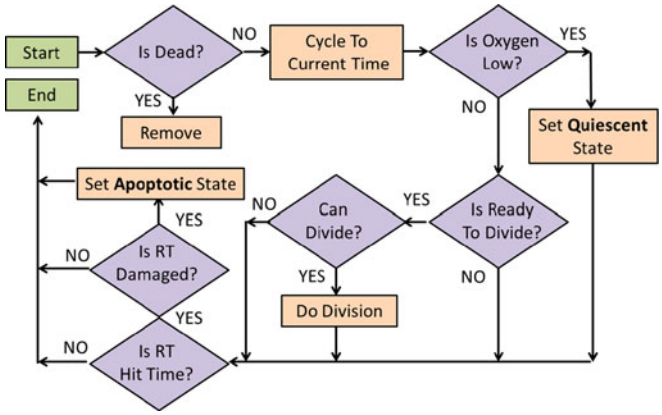


Fig. 3. Schematic of the algorithm used to update the cell population on each timestep, including RT administration.

cell [20]. The delta function $\delta(\mathbf{x})$ is unity at cell centers and zero elsewhere. No flux of oxygen is permitted through any of the planar faces of the bounding cuboid. Vessels act as constant sources of oxygen. Each point on the PDE grid which coincides with a vessel is prescribed a fixed oxygen tension of 30 mmHg, by means of a point-wise Dirichlet boundary condition.

Following the model preprocessing steps, the cell population and oxygen field are updated at each time increment, of duration 1.0 h, while the vasculature is static. The detailed cell update is shown in Fig. 3. "Normoxic" cells pass through a cell cycle, according to a model described in detail in Owen *et al.* [20]. In particular, a scalar parameter $0 \leq \phi \leq 1$ is used to describe a cell's progress through its cycle via

$$\frac{d\phi}{dt} = \frac{1}{T_{\min}} \frac{c}{(c_\phi + c)}, \tag{2}$$

where the cycle starts at $\phi = 0$ and ends, with attempted division, when $\phi = 1$, $T_{\min}$ is the minimum period of the cell cycle in oxygen rich conditions and $c_\phi$ is the oxygen tension at which the rate of progression through the cycle is half-maximal. Cells become quiescent and no longer cycle if the oxygen tension falls below a threshold value ($c < c_q^i$). Quiescent cells may resume cycling if the oxygen tension increases sufficiently ($c > c_q^o$). If a cell remains quiescent for a time period greater than the threshold $T_q$, then it becomes apoptotic. When RT is delivered, a fraction of the proliferating cells $(1 - SF)$ become apoptotic, where $SF$, the survival fraction, depends on the local oxygen tension $c$ in the following way:

$$SF = e^{-\alpha D - \beta D^2} \tag{3}$$

where $D$ is the radiation dose (in Gy) and $\alpha = \alpha(c)$ and $\beta = \beta(c)$ are empirical, oxygen-dependent parameters given by:

$$\alpha(c) = \frac{\alpha_{\max}}{OER_\alpha(c)}, \quad \beta(c) = \frac{\beta_{\max}}{OER_\beta(c)}, \tag{4}$$

and the OER satisfies [21]

$$OER(c) = OER_{\min} + (OER_{\max} - OER_{\min}) \frac{K_{\mathrm{OER}}}{c + K_{\mathrm{OER}}} \tag{5}$$

TABLE I
SUMMARY OF MODEL PARAMETERS AND ESTIMATES OF THEIR VALUES

| Parameter | Symbol | Units | Value | Source |
|---|---|---|---|---|
| Effective diffusivity | $D_e$ | $\mathrm{cm}^2 \cdot \mathrm{min}^{-1}$ | 0.00145 | [20] |
| Oxygen consumption rate | $k$ | $\mathrm{min}^{-1}$ | 13 | [20] |
| Radiotherapy dose | $D$ | Gy | 2.0 | – |
| Radiotherapy parameter | $\alpha_{\max}$ | $\mathrm{Gy}^{-1}$ | 0.3 | [7] |
| Radiotherapy parameter | $\beta_{\max}$ | $\mathrm{Gy}^{-2}$ | 0.03 | [7] |
| Oxygen enhancement parameter | $\mathrm{OER}_{\alpha,\min}$ | – | 1 | [29] |
| Oxygen enhancement parameter | $\mathrm{OER}_{\alpha,\max}$ | – | 1.75 | [29] |
| Oxygen enhancement parameter | $\mathrm{OER}_{\beta,\min}$ | – | 1 | [29] |
| Oxygen enhancement parameter | $\mathrm{OER}_{\beta,\max}$ | – | 3.25 | [29] |
| Oxygen enhancement parameter | $K_{\mathrm{OER}}$ | mmHg | 3.28 | [29] |
| Minimum cell cycle duration | $T_{\min}$ | min | 1600 | [20] |
| Cell cycle rate constant | $c_\phi$ | mmHg | 1.4 | [20] |
| Quiescence entrance threshold | $c_q^i$ | mmHg | 8.9 | [20] |
| Quiescence exit threshold | $c_q^o$ | mmHg | 9.8 | [20] |
| Maximum quiescence duration | $T_q$ | min | 4000 | [20] |

where $OER_{\min}, OER_{\max}$, and $K_{\mathrm{OER}}$ are empirical constants. Apoptotic cells are set to a "Dead" state and no longer occupy space after a period of 30 h. The viable fraction of cells at time $t$, $VF(t)$, is defined to be the total number of "Normoxic" and "Quiescent" cells at time $t$ divided by the total number of cells at the start of the simulation ($t = 0$). This quantity is a model output, which is distinct from the $SF$ which is a model input, and includes loss of cells due to both RT and hypoxia.

### C. Study Overview

Tumor growth and RT were simulated for each of the three types of vessel network and for each of the three spatial representations of the vessel networks, using as default the parameter values stated in Table I. For comparison, control cases with no vessels ($c = 0$ mmHg at all points, "Low") and well oxygenated tissue ($c = 30$ mmHg at all points, "High") were also simulated. For all cases, five realizations of the "Random" network and five realizations of the 3-D "Regular" network were simulated. Additionally, RT ($D = 2$ Gy) was administered at $t = 2$ h and thereafter every 24 h over a period of five days. Treatment was then halted and the tumor allowed to regrow for a total simulation time of 200 h (just over eight days).

In all cases, the number of cells in each state and the mean cell oxygen tensions were recorded every five hours, with a simulation time increment of one hour and cell cycle time increment of 30 min adopted. Simulations were built using the C++ Chaste library [17] with Python-based bindings and post-processing, ordinary differential equation systems were solved using CVODE [6] and PDE systems using a finite-difference scheme implemented with PETSc tools [4]. Simulation clock time was between 30 s and five minutes on a single AMD-FX4350 processor.

## III. RESULTS

### A. Cell Growth and Response to RT

Typical simulation results for the 3-D and 2-D biological networks are presented in Fig. 4 and the associated summary

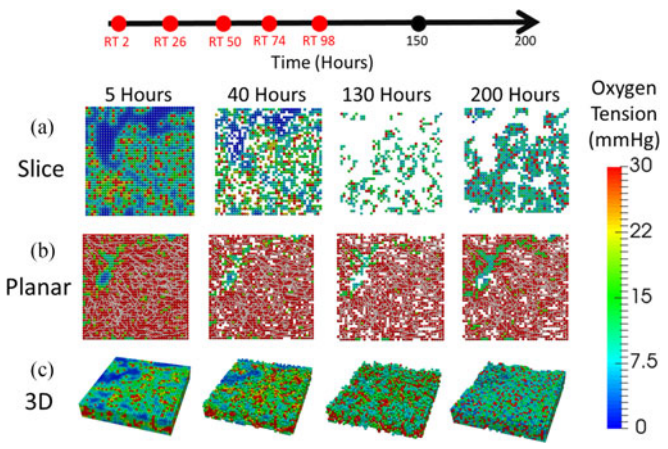


Fig. 4. Influence of geometry on cell growth and response to RT. Simulations at times $t = 5$, 40, 130 and 200 h, comparing the response of tumor cells embedded in (a) "Slice," (b) "Planar," and (c) the "3-D" representation of one of the biological networks to five rounds of daily RT. Administration times are also indicated. Cellular oxygen tension in mmHg is contoured. Parameter values: as per Table I, except for the oxygen consumption rate which is increased by a factor of 15 (from $k = 13$ min$^{-1}$ to $k = 195$ min$^{-1}$).

statistics are plotted in Fig. 5. Prior to RT, the 3-D tissue is densely populated with tumor cells that consume oxygen. As a result, the tissue is characterized by large regions with low oxygen and smaller, well-oxygenated regions. When RT is administered, due to the OER, well-oxygenated cells are killed at a greater rate than the poorly-oxygenated ones. As the tumor burden decreases, average oxygen levels rise and, as a result, the remaining cells become more vulnerable to RT. After 200 h (and five rounds of RT), the tumor cells repopulate the domain, causing the survival fraction (see (3)) to increase. The results for the 2-D simulations are similar, with progressively more tumor cell death for the 2-D "Planar" and "Slice" network representations. Given that the 2-D "Planar" network is better oxygenated than its 3-D counterpart, this suggests that, for the parameter values being used, the amount of cell death caused by RT is so great that it takes longer for the cells associated with the 2-D "Planar" network to repopulate the tissue than for the 3-D case where lower oxygen levels reduce the cell proliferation rate but have a stronger, inhibitory effect on radiosensitivity. An additional anomaly associated with the 2-D "Planar" representation is that tumor cells and their progeny must remain localized in finite regions surrounded by blood vessels. If all the tumor cells in one such region are eliminated following RT then that region will ever after remain devoid of tumor cells: this is not the case for the 2-D "Slice" or 3-D network representations.

### B. Effect of Vessel Morphology on Response to RT

The results presented in Fig. 5 reveal that, in 3-D, details of the microstructure of the vessel network have a negligible effect on the tumor's growth dynamics and/or its response to RT. There is good agreement between the predicted evolution of the average oxygen tension and the fraction of viable cells for 3-D simulations using the "Biological," "Random," and "Regular" networks. In particular, when the oxygen consumption rate is low [see Fig. 5(a)–(c)] the system dynamics can be accurately approximated by the "High" control case for which oxygen levels at all times are maintained at the same high levels throughout the tissue domain. Slight functional discrepancies between the different networks become apparent when the oxygen consumption rate is high [see Fig. 5(d)–(f)]. In this case, the biological network is typically better oxygenated than the synthetic ones, as shown in Fig. 5(d). It also has a lower proportion of hypoxic cells [see Fig. 5(c)] and, once RT stops, regrows more rapidly as shown in Fig. 5(f).

### C. Effect of Vessel Representation on Response to RT

The simulation results in Fig. 4 suggest that, for the biological network, the 2-D "Planar" representation does not accurately represent the 3-D one. These comparisons are made more precise in Fig. 6 where we plot the viable fraction, VF($t$), at two time points ($t = 5$, 95 h) for all vessel networks and two oxygen consumptions.

At early times, when the oxygen consumption rate is low, VF($t$) increases as the geometry changes from 3-D to 2-D "Planar" and 2-D "Slice" for the "Biological," "Random," and "Regular" networks, and a similar trend is seen for the two control cases [see Fig. 6(a)]. Since for the control cases, oxygen levels are identical for the 3-D and 2-D geometries, we ascribe this trend to undersampling: the 2-D domains contain significantly fewer cells than the 3-D domains so, for the 2-D simulations, there are fewer cells to sample when deciding whether a particular cell will survive RT. In future work, we will investigate this claim further by performing simulations on larger domains.

As the oxygen consumption rate increases [see Fig. 6(b)], or at later times [see Fig. 6(c)], the influence of geometry on the cells' response to RT becomes more apparent. Relative to a particular 3-D network, the "Slice" representation overestimates the VF whereas the "Planar" representation underestimates it. Fig. 4 reveals that these differences are due to the "Planar" ("Slice") representation supplying more (less) oxygen to the cells than the 3-D representation and, thereby, increasing (decreasing) the cell kill rate on exposure to RT.

An interesting anomaly is observed between the 3-D and 2-D "Slice" network representations. At early times (5 h), average hypoxic fractions for the 2-D "Slice" (0.41) are significantly higher for the "Biological" network than for the 3-D representation (0.17). Fractions in the "Random" network are similar for the "Slice" (0.18) and 3-D case (0.20), while fractions in the "Regular" network are underestimated in the "Slice" (0.05) relative to the 3-D case (0.20). Although the hypoxic fractions are quite different, the predicted mean oxygen tensions in each representation are reasonably similar (9.0, 13.9, and 16.3 mmHg for the "Slice" representation of the "Biological," "Random," and "Regular" networks, respectively and 14.2, 12.9, and 11.5 mmHg for the corresponding 3-D representations). The greater hypoxic fraction in the 2-D "Biological" network leads to a reduced initial RT response, as shown in Fig. 7, followed by a rapid reduction in VF as hypoxic cells start to die at $t \simeq 60$ h. This is the timescale associated with apoptosis of the

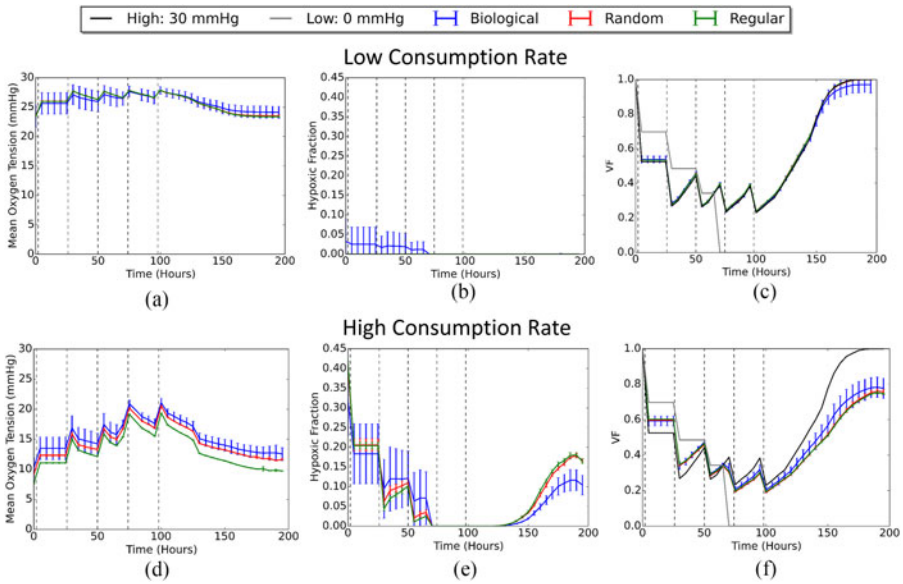


Fig. 5. Influence of vessel network representation on tumor cell growth and response to RT. Subplots show (a) the predicted mean cell oxygen tension, (b) hypoxic fraction of cells ($c < 5$ mmHg) and (c) viable fraction of cells over time, respectively, for the lower oxygen consumption rate ($k = 13$ min$^{-1}$) in 3-D vessel networks. Subplots (d)–(f) show the corresponding results for a consumption rate which is 15 times higher ($k = 195$ min$^{-1}$). Also included are results from "Low" and "High" controls where oxygen tensions are held fixed at 0 mmHg and 30 mmHg respectively at all points in the domain. The vertical dashed lines indicate RT administration times.

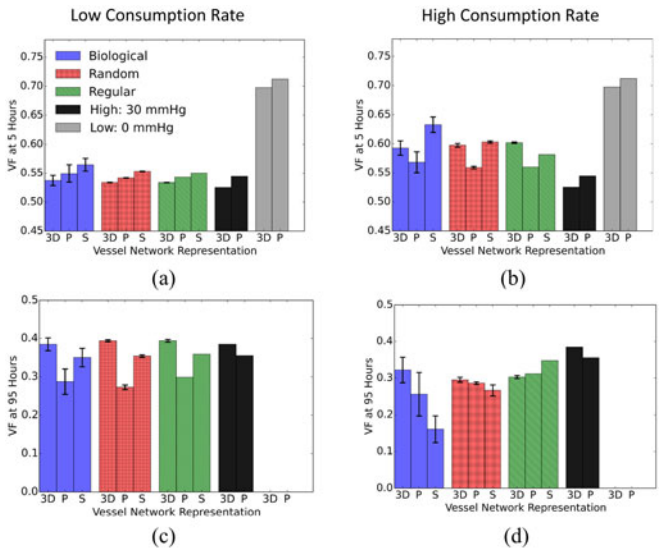


Fig. 6. Influence of geometry and vessel network representation on tumor response to RT. Cell survival fractions at $t = 5$ h for (a) the default oxygen consumption rate ($k = 13$ min$^{-1}$) and (b) a high oxygen consumption rate ($k = 195$ min$^{-1}$). Corresponding results at $t = 95$ h are presented in (c) and (d). Key: 3-D-"3-D" Network, P-"Planar," S-"Slice."

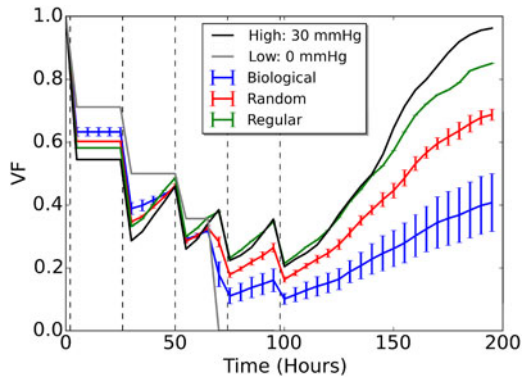


Fig. 7. Predicted cell viable fraction for the 2-D "Slice" vessel network. Vertical dashed lines indicate RT administration times. Parameter values: as per Table I, except oxygen consumption rate which is fixed at a high level ($k = 195$ min$^{-1}$).

quiescent cells that the low oxygen environment creates. The additional cell death due to oxygen deprivation results in the considerably lower viable fraction predicted by the "Slice" representation of the "Biological" network than the others, as shown in Fig. 6(d). This greater hypoxic fraction in the "Slice" network may be due to heterogeneity in the vessel spacing, which is most evident in the "Biological" network. The predictions of the 2-D "Slice" representation thus appear to have greater sensitivity to spatial heterogeneity in the vessel distribution than the 3-D representation.

## IV. Discussion

We have used a hybrid, multiscale model to investigate how the representation of microvascular networks influences tissue oxygenation and the response of tumors to multiple rounds of RT. Numerical simulations in 3-D reveal no significant differences for the three network types under consideration, although it is noted that the studied biological network is relatively well vascularized. If oxygen consumption rates are low, then details of the microvascular structure in the case of well vascularized tumors can be ignored and the tumor's growth dynamics and response to RT is reasonably predicted by assuming that tissue

oxygen levels are constant in space and time. As the oxygen consumption rate increases, this approximation ceases to apply as mean oxygen levels change over time [see Fig. 5(a) and (d)]. Based on these results, we conclude that, when predicting tumor growth and response to RT, details of the vasculature supplying oxygen to the tumor should be taken into consideration but that biological structure for this well vascularized case can be reasonably approximated by an equivalent "Random" or "Regular" network.

Our 3-D simulations provide a detailed description of oxygen transport in tumor regions that are small (1.6 mm $\times$ 1.6 mm $\times$ 0.28 mm) relative to human tumor sizes. In practice, when simulating the treatment of patients in the clinic, larger tissue regions should be considered. Homogenization techniques can be used to relate bulk or macroscale properties of vascular tumors to their microscale structure [31]. Our analysis reveals that assuming a regular or periodic distribution of vessels at the microscale, which greatly simplifies the upscaling analysis, will yield predictions for oxygen transport at the tissue scale that will be similar to those generated from the underlying biological network.

Comparison of simulation results for the 3-D and 2-D geometries suggests that care is needed when extrapolating results from 2-D approximations to 3-D. In more detail (and as illustrated in Figs. 4 and 5), the 2-D "Slice" representations of the networks tend to overestimate viable tumor cell numbers at early times and to underestimate them at later times. By contrast, the 2-D "Planar" representation of the vessel networks consistently overestimates the cell kill following RT. There are several reasons for these discrepancies. First, the vessel volume fraction associated with 2-D "Planar" representations overestimates that of the 3-D network while the 2-D "Slice" representation underestimates it. For the 2-D "Planar" representation, when vascular remodeling or multiple occupancy for lattice points [20] are neglected, tumor cells may get trapped in sub-regions of the tissue that are enclosed by blood vessels—if all tumor cells in such a region are eliminated, that region will always remain devoid of tumor cells.

Our results correspond to relatively small tumor regions (less than 1 $mm^3$) that are reasonably homogeneous, due to the choice of cell line and use of a mouse model. When studying tumor growth in humans, larger tissue regions should be considered and these may encompass larger scale (intratumoral) heterogeneities, with subregions of hypoxia, necrosis, and normoxia coexisting in a given tissue region. Scott *et al.* [29] studied larger tissue regions in a similar study and predicted that at low vessel densities, radiation efficacy decreased when the vessels were uniformly distributed, whereas at high vessel densities, radiation efficacy increased when the vessels were uniformly distributed. We conclude that when relating macroscale properties of tumor tissue to microscale features, a key challenge is to correctly define the size of the microscale regions. It is noted from Fig. 6(d) that the predicted viable fraction in the 2-D "Slice" representations is more sensitive to heterogeneities in the vessel distribution between the "Regular" and "Random" networks than the 3-D representations. This suggests that further study is also required into the sensitivity of point-wise representations of vessel networks to spatial heterogeneities relative to 3-D descriptions.

The relatively sparse cell spacing of 40 $\mu$m used in this study should be reduced to more closely resemble the packing of cancer cells in 3-D, as is investigated in the study of Owen *et al.* [20], who allowed for multiple cell occupancy at lattice sites. This is feasible with the present model, as with careful interpolation of vessel locations onto the regular lattice, simulation times are expected to scale approximately linearly with cell number. It is noted, however, that one of the main outcomes of such a spatially uniform increase in cell numbers is an increased average oxygen consumption rate. This has already been explored in the present study by increasing the oxygen consumption rate by a factor of 15. Some further insights into how predictions depend on model inputs in Table I can be gained based only on this change in oxygen consumption rate. For example, parameters increasing the drop in oxygen tension between vessels, or dependence of RT surviving fraction on oxygen tension, are expected to exacerbate differences in predicted viable fractions post RT. A more formal, global, sensitivity analysis [15] would be beneficial for a more detailed exploration of the role of parameters in Table I and to assess prediction robustness to parameter changes. This should be feasible given the relatively short simulation times in this study, but is postponed to future work.

Like Scott *et al.* [29], our simulation results are derived from static vascular networks that supply oxygen to the tumor tissue at a constant rate. In future work, we will investigate how our results change when effects such as tumor blood flow, angiogenesis, and vascular remodeling are incorporated. While models of these processes have been implemented in existing multiscale models of vascular tumor growth (for example [16], [19], [20]), they have not been validated against suitable experimental data. In future work, we aim to use *in vitro* and *in vivo* measurements of red blood cell transport through realistic tumor networks and measurements of micro-vasculature evolution [25], [33] to develop and validate mathematical models for these processes. We will use the validated models to investigate the impact of vessel normalization strategies on tumor responses to RT [13] and to determine how different treatments (*e.g.* chemotherapy and immunotherapy) should be coordinated with RT and personalized for individual patients.

## V. Conclusion

We have implemented a hybrid, multiscale model of vascular tumor growth and used it to investigate how the microscale description of the vessel network influences tissue oxygenation and the tumor's response to RT. No significant differences in either tissue oxygen levels or tumor burden were observed when 3-D simulations were generated from "Biological," "Random," and "Regular" vessel networks. Tumor growth dynamics in each case were in good agreement with results generated from simulations in which a spatially uniform oxygen distribution was imposed across the tissue domain. Comparison of results from 3-D and 2-D simulations revealed that 2-D "Slices" through the 3-D vasculature provide a better approximation to the 3-D network than 2-D "Planar" representations. This is because oxygen

tension is not overestimated and lattice occupancy artifacts are not introduced. However, "Slices" overestimated cell death in certain cases when oxygen consumption rates were high. Implicit in these conclusions are two key modeling assumptions: 1) oxygen levels are maintained at constant levels at all points within the vessel network and 2) the vessel network is not subject to remodeling. Future work is focused on relaxing these assumptions, with the ultimate aim of establishing how vessel normalization strategies should be administered to maximize the therapeutic efficacy of RT.

## REFERENCES


[1] M. D. Abramoff, "Image processing with ImageJ," *Biophoton. Int.*, vol. 11, no. 7, pp. 36–42, 2004.

[2] T. Alarcon, "A cellular automaton model for tumour growth in inhomogeneous environment," *J. Theoretical Biol.*, vol. 225, no. 2, pp. 257–74, 2003.

[3] T. Alarcon, "A multiple scale model for tumor growth," *Multiscale Modeling Simul.*, vol. 3, no. 2, pp. 440–475, 2005.

[4] S. Balay, "PETSc user's manual revision 3.5," Argonne Nat. Laboratory, Lemont, IL, USA, Tech. Rep. ANL-95/11, 2014.

[5] A. C. Begg, "Predicting recurrence after radiotherapy in head and neck cancer," *Seminars Radiation Oncol.*, vol. 22, no. 2, pp. 108–118, 2012.

[6] S. D. Cohen and A. C. Hindmarsh, "PCVODE, a stiff/nonstiff ODE solver in C," *Comput. Phys.*, vol. 10, no. 2, pp. 138–43, 1996.

[7] A. Dasu, "Theoretical simulation of tumour oxygenation and results from acute and chronic hypoxia," *Phys. Med. Biol.*, vol. 48, no. 17, pp. 2829–2842, 2003.

[8] A. Dasu, "The effects of hypoxia on the theoretical modelling of tumour control probability," *Acta Oncol.*, vol. 44, no. 6, pp. 563–571, 2005.

[9] H. Enderling, "Quantitative modelling of tumour dynamics and radiotherapy," *Acta Biotheoretica*, vol. 58, no. 4, pp. 341–353, 2010.

[10] D. R. Grimes, "Estimating oxygen distribution from vasculature in three-dimensional tumor tissue," *J. Roy. Soc. Interface*, vol. 13, no. 116, 2016, Art. no. 20160070.

[11] L. Hlatky, "Clinical application of antiangiogenic therapy: Microvessel density, what it does and doesn't tell us," *J. Nat. Cancer Inst.*, vol. 94, no. 12, pp. 883–893, 2002.

[12] M. R. Horsman and J. Overgaard, "The impact of hypoxia and its modification of the outcome of radiotherapy," *J. Radiation Res.*, vol. 57, pp. i90–i98, 2016.

[13] R. K. Jain, "Normalisation of tumour vasculature: An emerging concept in antiangiogenic therapy," *Science*, vol. 307, no. 5706, pp. 58–62, 2005.

[14] H. Kempf, "Spatio-temporal cell dynamics in tumour spheroid irradiation," *Eur. Phys. J. D*, vol. 60, no. 1, pp. 177–193, 2010.

[15] S. Marino, "A methodology for performing global uncertainty and sensitivity analysis in systems biology," *J. Theoretical Biol.*, vol. 254, no. 21, pp. 178–196, 2008.

[16] S. R. McDougall, "Mathematical modelling of flow through vascular networks: implications for tumour-induced angiogenesis and chemotherapy strategies," *Bulletin Math. Biol.*, vol. 64, no. 4, pp. 673–702, 2002.

[17] G. R. Mirams, "Chaste: An open source C++ library for computational physiology and biology," *PLoS Comput. Biol.*, vol. 9, no. 3, 2013, Art. no. e1002970.

[18] J. Overgaard and M. R. Horsman, "Modification of hypoxia-induced radioresistance in tumours by the use of oxygen and sensitizers," *Seminars Radiation Oncol.*, vol. 6, no. 1, pp. 10–21, 1996.

[19] M. R. Owen, "Angiogenesis and vascular remodelling in normal and cancerous tissues," *J. Math. Biol.*, vol. 58, no. 4/5, pp. 689–721, 2009.

[20] M. R. Owen, "Mathematical modelling predicts synergistic antitumour effects of combining a macrophage-based, hypoxia-targetted gene therapy with chemotherapy," *Cancer Res.*, vol. 71, no. 8, pp. 2826–2837, 2011.

[21] B. Palcic and L. D. Skarsgard, "Reduced oxygen enhancement ratio at low doses of ionizing radiation," *Radiation Res.*, vol. 100, no. 2, pp. 328–339, 1984.

[22] H. Perfahl, "Multiscale modelling of vascular tumour growth in 3D: The roles of domain size and boundary conditions," *PLoS One*, vol. 6, no. 4, 2011, Art. no. e14790.

[23] A. S. Popel, "Analysis of capillary-tissue diffusion in multicapillary systems," *Math. Biosci.*, vol. 39, pp. 187–211, 1978.

[24] G. G. Powathil, "Towards predicting the response of a solid tumour to chemotherapy and radiotherapy treatments: Clinical insights from a computational model," *PLoS Comput. Biol.*, vol. 9, no. 7, 2013, Art. no. e1003120.

[25] A. R. Pries, "Blood flow in microvascular networks. Experiments and simulation," *Circulation Res.*, vol. 67, no. 4, pp. 826–834, 1990.

[26] R. Rockne, "A mathematical model for brain tumour response to radiation therapy," *J. Math. Biol.*, vol. 58, no. 4/5, pp. 561–578, 2009.

[27] R. C. Rockne, "A patient-specific computational model of hypoxia-modulated radiation resistance in glioblastoma using 18F-FMISO-PET," *J. Roy. Soc. Interface*, vol. 12, no. 103, 2015, Art. no. 20141174.

[28] K. E. Schlageter, "Microvessel organisation and structure in experimental brain tumours: Microvessel populations," *Microvascular Res.*, vol. 58, no. 3, pp. 312–328, 1999.

[29] J. G. Scott, "Spatial metrics of tumour vascular organisation predict radiation efficacy in a computational model," *PLOS Comput. Biol.*, vol. 12, no. 1, 2016, Art. no. e1004712.

[30] T. W. Secomb, "Analysis of oxygen transport to tumor tissue by microvascular networks," *Int. J. Radiation Oncol. Biol. Phys.*, vol. 25, no. 3, pp. 481–489, 1993.

[31] R. J. Shipley and S. J. Chapman, "Multiscale modelling of fluid and drug transport in vascular tumours," *Bulletin Math. Biol.*, vol. 72, no. 6, pp. 1464–1491, 2010.

[32] R. M. Sutherland and R. E. Durand, "Radiation response of multicell spheroids—An in vitro tumour model," *Current Topics Radiation Res. Quart.*, vol. 11, no. 1, pp. 87–139, 1976.

[33] G. M. Tozer, "Intravital imaging of tumour vascular networks using multi-photon fluorescence microscopy," *Adv. Drug Del.*, vol. 57, pp. 135–152, 2005.

[34] M. Welter and H. Rieger, "Physical determinants of vascular network remodeling during tumor growth," *Eur. Phys. J. E, Soft. Matter*, vol. 33, no. 2, pp. 149–163, 2010.


Authors' photograph and biography not available at the time of publication.